Growth and Decay of a Convective Boundary Layer over a Surface with a Constant Temperature

CHIEL C. VAN HEERWAARDEN AND JUAN PEDRO MELLADO

Max Planck Institute for Meteorology, Hamburg, Germany

(Manuscript received 19 October 2015, in final form 18 February 2016)

ABSTRACT

The growth and decay of a convective boundary layer (CBL) over a surface with a constant surface temperature that develops into a linear stratification is studied, and a mathematical model for this system is derived. The study is based on direct numerical simulations with four different Reynolds numbers; the two simulations with the largest Reynolds numbers display Reynolds number similarity, suggesting that the results can be extrapolated to the atmosphere. Because of the interplay of the growing CBL and the gradually decreasing surface buoyancy flux, the system has a complex time evolution in which integrated kinetic energy, buoyancy flux, and dissipation peak and subsequently decay. The derived model provides characteristic scales for bulk properties of the CBL. Even though the system is unsteady, self-similar vertical profiles of buoyancy, buoyancy flux, and velocity variances are recovered. There are two important implications for atmospheric modeling. First, the magnitude of the surface buoyancy flux sets the time scale of the system; thus, over a rough surface the roughness length is a key variable. Therefore, the performance of the surface model is crucial in large-eddy simulations of convection over water surfaces. Second, during the phase in which kinetic energy decays, the integrated kinetic energy never follows a power law, because the buoyancy flux and dissipation balance until the kinetic energy has almost vanished. Therefore, the applicability of power-law decay models to the afternoon transition in the atmospheric boundary layer is questionable; the presented model provides a physically sound alternative.

1. Introduction

This paper addresses the growth and decay of a convective boundary layer (CBL) over a surface with a constant surface temperature. Few studies exist of the basic properties of such a boundary layer; most of the simulation-based studies of the properties of the turbulent flow in the CBL have been done using a fixed surface flux (e.g., Moeng 1984; Sullivan et al. 1998; Fedorovich 1995; Garcia and Mellado 2014), whereas many of the studies with a fixed surface temperature address cloudy boundary layers over sea, often in a setting including radiative cooling (e.g., Tompkins and Craig 1998; vanZanten et al. 2011).

Our study of a CBL over a fixed-temperature surface has relevant applications. It represents, for instance, a limiting case of the decay of turbulence in the CBL: one where the system dies out very slowly. Furthermore, it can help in understanding heterogeneously heated and cooled boundary layers over sea ice; here, it represents the limiting case of a boundary layer that forms over a very wide Arctic lead (Esau 2007). It also represents an idealized setting to study the reaction of a CBL over sea to changes in the sea surface temperature.

In this paper, we study this CBL in one of its most simple forms: the growth of a CBL against a linear stratification over a surface with a fixed temperature, without a balancing cooling force and without a large-scale horizontal pressure force and subsidence. This system develops and dies out over time, as the atmospheric buoyancy evolves toward that of the surface, resulting in an unsteady system with a vanishing near-surface gradient. Our aim is to derive a mathematical model for the system in order to find the relevant time scales as a function of the external parameters. This model is verified against direct numerical simulations (DNSs) of the system. The motivation for using DNS is that it does not require us

Corresponding author address: Chiel C. van Heerwaarden, Wageningen University, P.O. Box 47, 6700 AA Wageningen, Netherlands.
E-mail: chiel.vanheerwaarden@wur.nl

DOI: 10.1175/JAS-D-15-0315.1

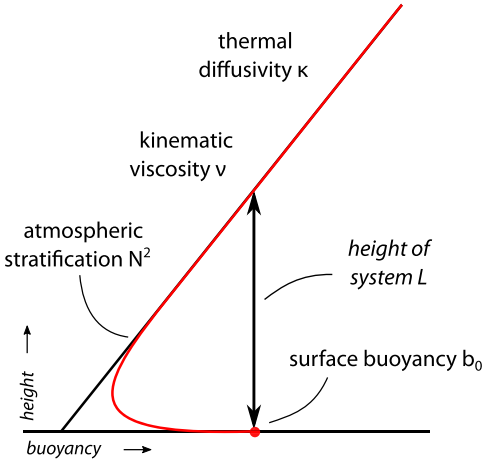

FIG. 1. Sketch of the system and its parameters. The red line illustrates a typical CBL during the initial development.

to use a surface model, as its applicability in a turbulence resolving model under conditions of free convection is still under discussion (Zilitinkevich et al. 2006; Mellado et al. 2015). As the Reynolds numbers acquired in direct numerical simulations are several orders of magnitude smaller than those in the atmosphere, this study contains a careful assessment of whether the results can be extrapolated to the atmosphere.

The organization of this paper is the following: In section 2, we define the system and apply dimensional analysis to minimize the number of independent parameters and to obtain first estimates of characteristic scales. Subsequently, we describe the simulation setup in section 3 and study the evolution of the system based on the simulations in section 4. In section 5, we propose a mathematical model that describes the evolution of the system as a function of time and derive the analytical solutions, which we verify against the simulations in section 6. In this analysis, we explore the presence of self-similarity and Reynolds number similarity. This is followed by a discussion on the applicability of the results to the atmosphere in section 7, including a discussion on the importance of surface roughness and of the relevance of this case to the study of the decay of turbulence during the afternoon transition.

2. Physical model and dimensional analysis

The physical model being studied is a linearly stratified atmosphere with kinematic viscosity ν and thermal diffusivity κ that is heated from below by a surface with a constant temperature (Fig. 1). For generality, we make use of buoyancy as our thermodynamic variable. We define buoyancy in terms of virtual potential temperature as $b \equiv (g/\theta_{v0})(\theta_v - \theta_{0v})$, where θ_{v0} is the virtual temperature of the background stratification at the surface. The linearly stratified system at rest has thus a surface buoyancy of $0\,\mathrm{m\,s^{-2}}$. We express the initial linear stratification as parameter $N^2 \equiv db/dz$. In our simulation, we assign a surface buoyancy b_0 to the system that is larger than zero to trigger convection and thus the development of a CBL.

The system is described by its four parameters (ν, κ, N^2, b_0) and has length and time as dimensions; thus, two nondimensional parameters can be derived. We use κ and N^2 to make the system dimensionless to arrive at

$$\left\{\frac{\nu}{\kappa}, \left(\frac{b_0^{4/3}}{\kappa^{2/3}N^2}\right)^{4/3}\right\}, \tag{1}$$

where the former is the Prandtl number (Pr) and the latter a reference Reynolds number (Re), which we explain below. In this study, we assume the Prandtl number to be unity, which allows for several simplifications in the following dimensional analysis.

In order get a better physical understanding of the system and to scale it later on, we introduce a set of characteristic scales. First, we define an outer length scale L:

$$L \equiv \frac{b_0}{N^2}, \tag{2}$$

which is the height at which the buoyancy of the linearly stratified atmosphere equals the surface buoyancy (Fig. 1). This is the maximum size the system can achieve. Then, we define the surface buoyancy flux scale B:

$$B \equiv b_0^{4/3}\kappa^{1/3}, \tag{3}$$

following inner-layer scaling (Townsend 1959; Mellado 2012), where we assume that the influence of stratification is not felt in the surface layer. With the help of the previous two scales, we can define a velocity scale to normalize the velocity fluctuations caused by turbulence:

$$U \equiv B^{1/3}L^{1/3} = \frac{b_0^{7/9}\kappa^{1/9}}{N^{2/3}}, \tag{4}$$

following Deardorff (1970). With the defined length and velocity scales, one can rewrite the defined

Reynolds number according to the classical definition $\mathrm{Re} = UL\nu^{-1}$.

Now we define a reference Kolmogorov length scale η for this system, where we assume that the total dissipation in the system is a fraction, of order 1, of the surface buoyancy flux. This gives

$$\eta \equiv \frac{\kappa^{3/4}}{B^{1/4}} = \frac{\kappa^{2/3}}{b_0^{1/3}}, \tag{5}$$

where the unity value of the Prandtl number is used to substitute ν with κ. It follows that the Reynolds number is equal to the four-thirds power of the scale separation; thus, $\mathrm{Re} = (L\eta^{-1})^{4/3}$.

The last scale to be defined is the time scale of the system. This time scale is the characteristic time scale of the evolution of the system and is therefore different than that of the turbulent fluctuations LU^{-1}. We assume time scale T to be proportional to the time it takes to warm up the system from the initial linear stratification to buoyancy b_0 over height L. The total energy required is proportional to $(1/2)b_0L$, whereas the speed at which it warms is proportional to the surface buoyancy flux such that we can define the time scale as

$$T \equiv \frac{b_0 L}{B} = \frac{b_0^{2/3}}{N^2 \kappa^{1/3}}. \tag{6}$$

To diagnose the actual state of the system, we define a length scale and a buoyancy scale that can be acquired from the vertical profile of horizontally averaged buoyancy $\langle b \rangle$. These are the required variables for the derivation of a mathematical model in section 5. Note that, in the remainder of this paper, horizontally averaged quantities are denoted with angle brackets. The scales are

$$h_*^2 \equiv \frac{2}{N^2} \int_0^\infty \langle b \rangle - N^2 z \, dz, \tag{7}$$

where

$$b_{\mathrm{ML}} \equiv \min(\langle b \rangle). \tag{8}$$

The definition of length scale h_* follows the same geometrical reasoning as that of time scale T. The total added energy is the equal to the integral in Eq. (7). If this integral is assumed to be a right triangle with legs h_* and $h_* N^2$, then normalization of the integral in Eq. (7) with $2N^{-2}$ gives the value of h_*^2. The time evolution of h_*^2 can be described by the following equation, where we make use of the governing equation for buoyancy to substitute the partial time derivative of buoyancy:

$$\begin{aligned} \frac{dh_*^2}{dt} &= \frac{2}{N^2} \frac{d}{dt} \left(\int_0^\infty \langle b \rangle - N^2 z \, dz \right) \\ &= \frac{2}{N^2} \left(\int_0^\infty \frac{\partial \langle b \rangle}{\partial t} dz \right) \\ &= \frac{2}{N^2} \left(\kappa \frac{\partial \langle b \rangle}{\partial z} \bigg|_\infty - \kappa \frac{\partial \langle b \rangle}{\partial z} \bigg|_0 \right) \\ &= \frac{2}{N^2} (\kappa N^2 + \langle B_s \rangle), \end{aligned} \tag{9}$$

where $\langle B_s \rangle$ is the time-varying horizontally averaged surface buoyancy flux.

With the latter equation, we have an exact evolution equation for our defined length scale h_*. We can rewrite Eq. (9) as an evolution equation for h_* that is, under the assumption that the buoyancy in the mixed layer is well-mixed, equivalent to a mixed-layer model that describes the evolution of the depth of a CBL that grows through encroachment:

$$\frac{dh_*}{dt} = \frac{\langle B_s \rangle + \kappa N^2}{h_* N^2}. \tag{10}$$

With the set of scaling variables $\{L, T, B\}$, we can rewrite Eq. (10) in terms of nondimensional variables. We define $\hat{h}_* \equiv h_*/L$, $\hat{t} \equiv t/T$, and $\hat{B}_s \equiv B_s/B$. Substitution into Eq. (10) results in the equivalent evolution equation:

$$\frac{d\hat{h}_*}{d\hat{t}} = \frac{\langle \hat{B}_s \rangle + \mathrm{Re}^{-3/4}}{\hat{h}_*}. \tag{11}$$

In section 5, we use Eq. (11) as the reference for the derivation of a mathematical model of the system for high–Reynolds number flows.

3. Numerical simulations

a. Formulation and model description

The evolution of the system is described by the set of evolution equations for velocity vector u_i, buoyancy b, and volume, formulated in flux form for a Boussinesq fluid:

$$\begin{aligned} \frac{\partial u_i}{\partial t} + \frac{\partial u_j u_i}{\partial x_j} &= -\frac{\partial \pi}{\partial x_i} + \delta_{i3} b + \nu \frac{\partial^2 u_i}{\partial x_j^2}, \\ \frac{\partial b}{\partial t} + \frac{\partial u_j b}{\partial x_j} &= \kappa \frac{\partial^2 b}{\partial x_j^2}, \\ \frac{\partial u_j}{\partial x_j} &= 0, \end{aligned} \tag{12}$$

where π is a modified pressure.

TABLE 1. Overview of the numerical simulations.

Name	$N_x \times N_y \times N_z$	b_0 (m s^{-2})	L (m)	ν, κ (m^2 s^{-1})	Re	t_{end} (s)
ReS	$1024 \times 1024 \times 384$	0.5	0.1667	1×10^{-5}	1876	400
ReM	$1024 \times 1024 \times 768$	1.0	0.3333	1×10^{-5}	6431	900
ReL	$1536 \times 1536 \times 768$	1.6	0.5333	5×10^{-6}	27 463	700
ReXL	$2048 \times 2048 \times 1024$	2.0	0.6667	5×10^{-6}	40 835	343

The velocity boundary conditions are specified as no penetration ($w = 0$) and no slip ($u = v = 0$) at the bottom boundary and no penetration and free slip ($\partial u/\partial z = \partial v/\partial z = 0$) at the top. The top boundary condition for buoyancy is a fixed gradient equal to the stratification N^2. The initial fields for velocity are set to zero, whereas the initial buoyancy profile is zero at the surface and increases with a constant gradient N^2 with height. Random noise is superimposed on the velocity fields in order to provide perturbations that trigger convection. The noise exponentially decays with height and is negligible beyond $0.1L$.

We use MicroHH (http://microhh.org), which is a 2D-parallel combined DNS/LES code. Fully conservative, fourth-order-accurate finite-difference schemes (Morinishi et al. 1998; Vasilyev 2000) have been used, combined with a low-storage third-order Runge–Kutta time integration scheme (Williamson 1980). The pressure is acquired by solving a Poisson equation. Here, the horizontal dimensions are decoupled using a Fourier decomposition, and for each mode a heptadiagonal matrix is solved. In the top of the domain (upper 25%) a damping layer is applied that prevents the reflection of gravity waves back into the domain with a damping time scale that is infinity at the bottom boundary of the damping layer and decreases exponentially to $(2\pi)/N$ at the top of the domain.

b. Numerical experiments

The results in this study are based on four direct numerical simulations, with varying Reynolds number and an identical Prandtl number of unity (Table 1). Each simulation has been run at a horizontal domain size of 2 m, with a linear stratification N^2 of 3 s^{-2}. The variations in the Reynolds number are acquired by varying the surface buoyancy b_0 and the thermal diffusivity κ. As the acquired boundary layer height is well approximated by b_0/N^2, the width-to-height aspect ratio reduces with Reynolds number from 12 in simulation ReS to 3 in simulation ReXL. The total runtime has been specified in Table 1. Note that ReXL could not be continued because of the small aspect ratio and the imminent reorganization of the flow into a single large-scale circulation.

4. Results

a. Characteristics

We first study the general characteristics of our system from the time evolutions of buoyancy- and kinetic-energy-related variables (Fig. 2). To already give an impression of the performance of the later-to-be-derived model, we have added its results with dotted black lines. Our analyses are partly based on the time evolution of several vertically integrated quantities that are denoted as I_ϕ, where ϕ is an arbitrary variable. The value of I_ϕ is calculated following

$$I_\phi \equiv \int_0^\infty \langle \phi \rangle \, dz . \tag{13}$$

We make use of the integrals of $b - N^2 z$, of kinetic energy $e \equiv (1/2)(u'^2 + v'^2 + w'^2)$, of the buoyancy flux $w'b'$, and of dissipation ε, denoted as I_b, I_e, I_B, and I_ε, respectively, where I_b is referred to as the vertically integrated buoyancy hereinafter.

The time evolution of the mean surface buoyancy flux $\langle B_s \rangle$ (Fig. 2a) shows that the energy input from the surface is decreasing in time from the beginning of the simulations and converges toward zero. With the chosen scaling variables, the four simulations and the derived model collapse very well. The surface flux does not decay exponentially, nor does it follow a power law, because of the nonlinear relation between surface buoyancy flux and the buoyancy difference over the surface layer and the increasing CBL depth over time.

The time evolution of the boundary layer depth h_* (Fig. 2b), calculated following Eq. (7), shows a growth that levels off in time, with a growth rate proportional to the energy input to the system. The CBL depth of the simulations with low Reynolds numbers (ReS and ReM) keeps increasing, because a nonnegligible amount of energy is added to the system through diffusion of buoyancy down the linear stratification. As the importance of diffusion from the top boundary decreases with Reynolds number [see Eq. (11)], the simulations with a higher Reynolds number develop toward an asymptotic CBL depth of L. The time evolution of those simulations is well predicted by the model.

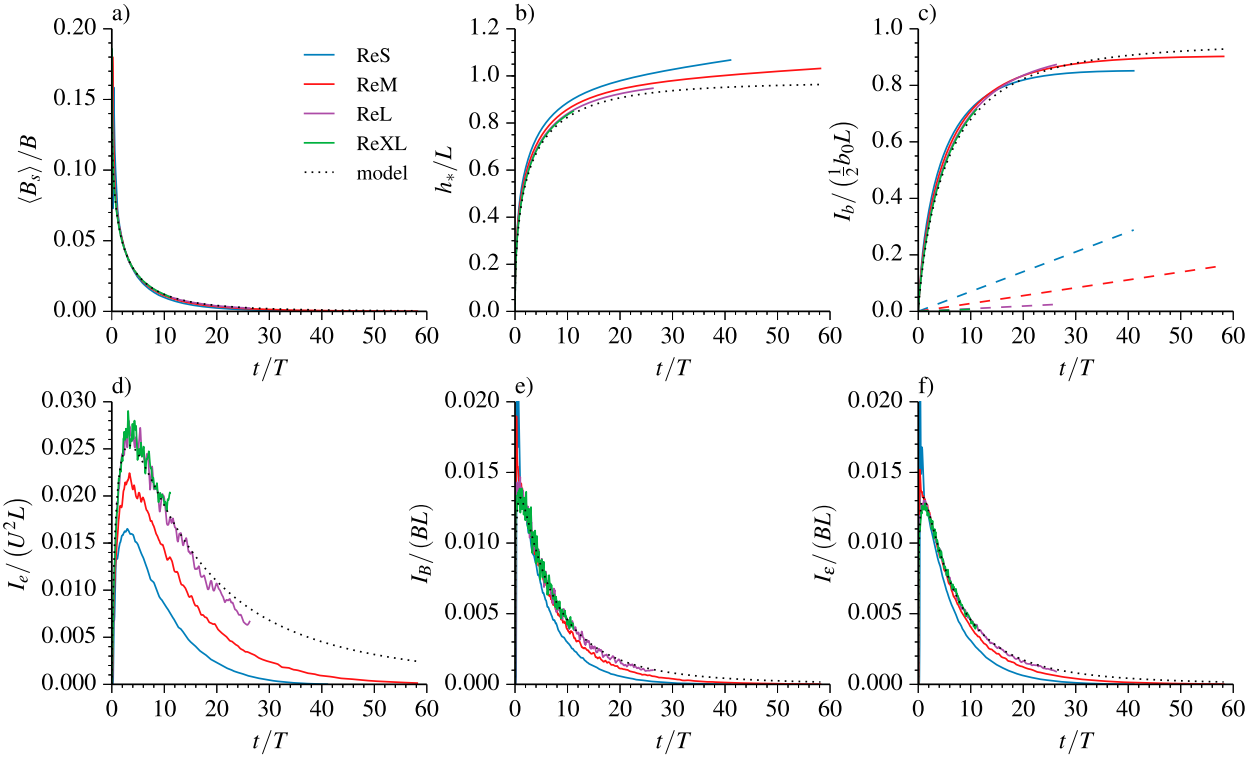

FIG. 2. (top) The nondimensional time evolution of (a) the mean surface buoyancy flux $\langle B_s \rangle$, (b) the boundary layer height h_*, and (c) the surface contribution to the vertically integrated buoyancy $I_b - \kappa N^2 t$ (solid line) and the top contribution to the vertically integrated buoyancy $\kappa N^2 t$ (dashed line). (bottom) The nondimensional time evolution of (d) the vertically integrated kinetic energy I_e, (e) buoyancy flux I_B, and (f) dissipation I_ε.

The time evolution of the vertically integrated mean buoyancy (Fig. 2c) shows two lines for each simulation: namely, the surface contribution to the integral, calculated as $I_b - \kappa N^2 t$ (solid lines), and the contribution of the top boundary $\kappa N^2 t$ (dashed lines). Each of the cases shows that the total amount of integrated buoyancy keeps increasing even when the surface buoyancy flux approaches zero. This is related to the molecular diffusion flux at the top of the domain. The results show that the molecular diffusion flux at the top becomes negligible at higher Reynolds numbers; already for case ReL the contribution is less than 3% at the end of the simulation. This means that the contribution of diffusion to the total heating can be neglected for the high–Reynolds numbers simulations. Therefore, our model approximates well the time evolution of the vertically integrated buoyancy and becomes progressively better for higher Reynolds numbers.

The time evolutions of vertically integrated mean kinetic energy, buoyancy flux, and dissipation (Figs. 2d–f) demonstrate the complexity of the system. The time evolution of the integrated kinetic energy (Fig. 2d) shows that there is first a phase in which the kinetic energy increases, during which the added potential energy through the surface buoyancy flux is converted into kinetic energy and the benefits of a deeper CBL outweigh the loss of buoyancy supply at the bottom boundary. The buoyancy flux and dissipation show a similar pattern, but with a peak that occurs earlier in time.

After the peak, the integrated variables decrease in time and slowly develop toward zero. Similar to the time evolution of the surface buoyancy flux, also the time evolution of the three kinetic-energy-related variables shows a complex decay pattern that is neither exponential nor follows a power law. With the model that we derive in section 5, we provide the proper algebraic scaling.

The derived model only predicts the correct kinetic energy for the two cases with the highest Reynolds numbers. Interestingly, the buoyancy flux and the dissipation are adequately predicted by the derived model in all four simulations. This suggests that, in the simulations with low Reynolds numbers (ReS and ReM), there is insufficient scale separation between the large scales at which the production happens and the smaller scales at which the energy is dissipated. Plumes are therefore already dissipated before they can reach their full potential, resulting in a lower integrated kinetic energy than in simulations ReL and ReXL.

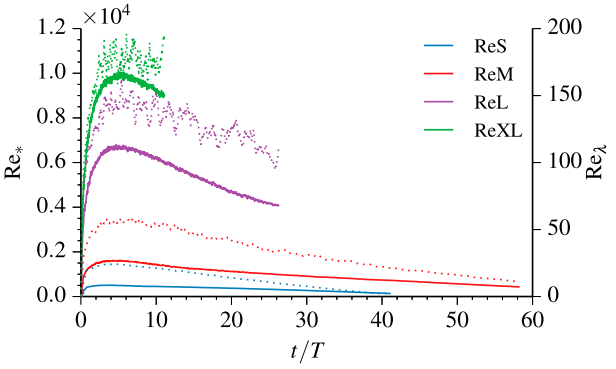

FIG. 3. Time evolution of the convective Reynolds number (Re_*; solid lines) and Taylor Reynolds number (Re_λ; dotted lines).

We conclude from the analysis that a high Reynolds number is a requirement for the study of the initial peak in integrated kinetic energy and, even more so, of those in the integrated buoyancy flux and dissipation. Only then is the time it takes to forget the initial perturbations and to form a fully turbulent layer sufficiently shorter than the time it takes to form the peak in kinetic energy so that the model is able to predict the integrated kinetic energy during the phase that its magnitude is still steeply increasing. The evolution toward the peak is thus not related to the spinup of the model, but is a fully physical process.

b. *Reynolds number*

Before the derivation of the mathematical model, we evaluate the Reynolds numbers of the simulations. In Fig. 3, the time evolution of two definitions of the Reynolds number is shown. The two are defined as

$$\mathrm{Re}_* \equiv B_s^{1/3} h_f^{4/3} \nu^{-1}, \tag{14}$$

$$\mathrm{Re}_\lambda \equiv \max\left\{\frac{[(2/3)\langle e\rangle]^{1/2}\lambda}{\nu}\right\} = \max\left[\left(\frac{20}{3}\frac{\langle e\rangle}{\langle\varepsilon\rangle\nu}\right)^{1/2}\right]. \tag{15}$$

The first is the convective Reynolds number (Re_*), and the second is the maximum in the vertical profile of the Taylor Reynolds number (Re_λ), as defined by Pope (2000, p. 200). In the latter, we substituted λ with $(10\nu\langle e\rangle\varepsilon^{-1})^{1/2}$ (Pope 2000, p. 199). Height h_f in Re_* is the height of the minimum in the mean buoyancy flux $\langle w'b'\rangle$. In terms of Re_λ, ReL has its peak at a value around 150 and decreases subsequently to values close to 100, whereas ReXL peaks close to 180. Both simulations fulfill the criteria of Dimotakis (2000) for fully developed turbulence, which sets an Re_λ of 100–140 as the threshold; thus, this corroborates our observation of Reynolds number similarity for simulations ReL and ReXL (Fig. 2).

To illustrate the influence of the Reynolds number on the flow characteristics, two cross sections of the surface buoyancy flux are displayed in Fig. 4. The left cross section shows simulation ReL at the moment of maximum Reynolds number, whereas the right one shows the state of that variable at the end of the simulation, where the Reynolds number has decreased considerably. The

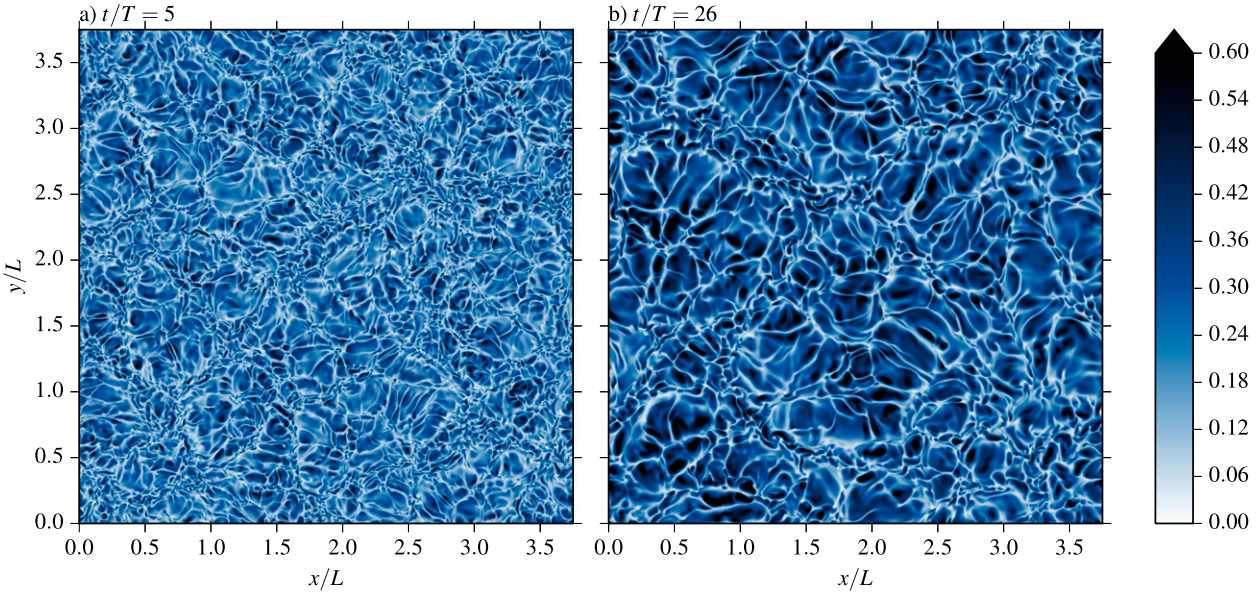

FIG. 4. The surface buoyancy flux B_s of the full computational domain (a) at its maximum Reynolds number ($t/T = 5$) and (b) at the end of the simulation ($t/T = 26$) for simulation ReL. The color scale ranges from no flux (white) to maximum flux (black). The scale is nonlinear and serves to highlight the flow structure the best.

decrease in Reynolds number reveals itself in the loss of small-scale features in the flow, as the size of the smallest eddies that can exist is increasing because of the decrease of energy input at the largest scales.

5. Mathematical model

a. Governing equations of the model

To create a mathematical model for the evolution of the system, we first need a model that describes the surface buoyancy flux, because we use a Dirichlet boundary condition. We make use of b_{ML} [Eq. (8)] and define the actual viscous length as $\delta \equiv \kappa^{2/3}(b_0 - b_{\mathrm{ML}})^{-1/3}$. Based on viscous scaling, we can define then the modeled surface buoyancy flux B_{sm}:

$$\langle B_s \rangle = -\kappa \frac{\partial \langle b \rangle}{\partial z}\bigg|_0 \approx B_{sm} \equiv c_0 \kappa \frac{b_0 - b_{\mathrm{ML}}}{\delta} = c_0 \kappa^{1/3}(b_0 - b_{\mathrm{ML}})^{4/3} \tag{16}$$

If we assume that B_{sm} is a good approximation for B_s, we can define a modeled length scale h_{*_m} according to Eq. (10), which is a good approximation for h_*. We make the conjecture that it takes a constant c_1 to relate b_{ML} to $h_{*_m} N^2$:

$$b_{\mathrm{ML}} = c_1 h_{*_m} N^2, \tag{17}$$

which we verify later.

This gives the following expression:

$$B_{sm} = c_0 \kappa^{1/3}(b_0 - c_1 h_{*_m} N^2)^{4/3}. \tag{18}$$

If we define $\hat{B}_{sm} \equiv B_{sm} b_0^{-4/3} \kappa^{-1/3}$, we acquire the following expression for the nondimensional surface buoyancy flux:

$$\hat{B}_{sm} = c_0 (1 - c_1 \hat{h}_{*_m})^{4/3}, \tag{19}$$

With Eq. (19) as the model for the surface buoyancy flux, we can define the differential equation that describes the evolution of the characteristic length scale h_{*_m} of the system. This equation is similar to Eq. (11), but under the assumption that the Reynolds number is so high that the top-diffusion term can be neglected:

$$\frac{d\hat{h}_{*_m}}{d\hat{t}} = \frac{c_0 (1 - c_1 \hat{h}_{*_m})^{4/3}}{\hat{h}_{*_m}}. \tag{20}$$

The constant c_0 has been discussed in detail in Beljaars (1995), where a similar dimensional analysis has been presented. This constant does not directly relate to a rough-wall scalar exchange coefficient, as these are generally applied in combination with a wind speed difference between the atmosphere and the surface, which we do not consider in our dimensional analysis. There are indications that such laws can be applied locally in free convection (Zilitinkevich et al. 2006), but this is still under debate. The analysis as we applied it can be extended to rough surfaces. To do so, we introduce a new modeled surface buoyancy flux B_{smR} that relates the flux to the roughness length z_0 and the buoyancy difference between z_0 and the mixed layer:

$$B_{smR} \equiv c_R z_0^{1/2} (b_{z_0} - b_{\mathrm{ML}})^{3/2}, \tag{21}$$

with a constant c_R to match the left- and right-hand side. The introduction of Eq. (21) into Eq. (10) gives, if we assume the high–Reynolds number limit, a model for the boundary layer depth over rough surfaces:

$$\frac{dh_{*_R}}{dt} = \frac{c_R z_0^{1/2} (b_{z_0} - c_1 h_{*_R} N^2)^{3/2}}{h_{*_R} N^2}, \tag{22}$$

which can be reduced to a similar form as Eq. (20), but with slightly different coefficients. Furthermore, this equation is not closed, as we also need theory and a model to describe the buoyancy at the roughness length b_{z_0}, which goes beyond the scope of this study.

b. Solutions of the governing equations

To solve Eq. (20) in its most general form, we define $\tilde{t} \equiv c_0 c_1^2 \hat{t}$ and $\tilde{h}_{*_m} \equiv c_1 \hat{h}_{*_m}$, which immediately shows that the characteristic time of the system is linearly related to c_0 and quadratically to c_1. The corresponding equation is

$$\frac{d\tilde{h}_{*_m}}{d\tilde{t}} = \frac{(1 - \tilde{h}_{*_m})^{4/3}}{\tilde{h}_{*_m}}. \tag{23}$$

This equation has the following implicit solution, which has been shown by Deardorff et al. (1969) and elaborated by Zilitinkevich (1991):

$$1 + \frac{2}{9}\tilde{t} = \frac{1}{3}(1 - \tilde{h}_{*_m})^{2/3} + \frac{2}{3}(1 - \tilde{h}_{*_m})^{-1/3}. \tag{24}$$

This function has a one-to-one mapping of t to h_{*_m} for $t \geq 0$ and $0 \leq h_{*_m} \leq 1$. We can distinguish two limiting cases. The first one is that, under the condition $\tilde{h}_{*_m} \ll 1$,

$$\frac{d\tilde{h}_{*_m}}{d\tilde{t}} \simeq \frac{1}{\tilde{h}_{*_m}}, \tag{25}$$

with solution

$$\tilde{h}_{*_m} \simeq (2\tilde{t})^{1/2}, \tag{26}$$

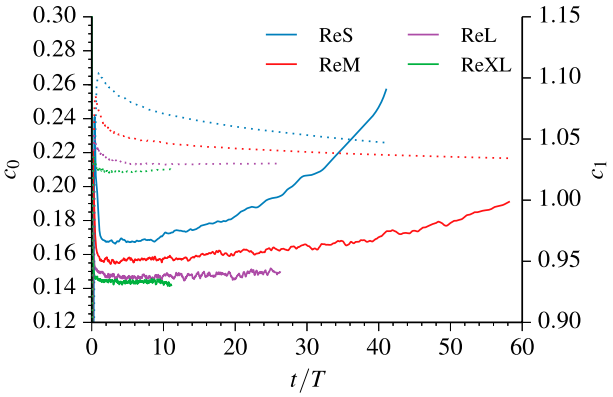

FIG. 5. Time evolution of $c_0 = \langle B_s \rangle (b_0 - b_{\mathrm{ML}})^{-4/3} \kappa^{-1/3}$ (solid lines) and $c_1 = b_{\mathrm{ML}} h_{*_m}^{-1} N^{-2}$ (dotted lines).

which is equal to the solution of the CBL with a fixed surface flux. This solution applies in the initial state, where the surface buoyancy has not reduced yet significantly as an effect of atmospheric warming.

The second limiting case is found in the approach of the final state, where $\tilde{h}_{*_m} \approx 1$:

$$\frac{d\tilde{h}_{*_m}}{d\tilde{t}} \simeq (1 - \tilde{h}_{*_m})^{4/3}. \tag{27}$$

This equation has solution

$$1 + \frac{1}{3}\tilde{t} \simeq (1 - \tilde{h}_{*_m})^{-1/3}, \tag{28}$$

which can be inverted to an expression for h_{*_m}:

$$\tilde{h}_{*_m} \simeq 1 - \left(\frac{3}{\tilde{t} + 3}\right)^3. \tag{29}$$

This solution describes the final state at which the nondimensional height of the system is approximately unity and only the variation in the surface buoyancy flux is still relevant. In our later discussion on the role of roughness in free convection (section 7), we make use of the approximated solutions. We complete our set of scaling variables by defining a convective velocity scale $w_{*_m} \equiv B_{sm}^{1/3} h_{*_m}^{1/3}$ (Deardorff 1970).

c. Fitting the constants

To apply this model for scaling the results, we need to fit the constants c_0 and c_1 based on the simulations. First, c_0 needs to be determined, as its value is required to infer c_1. The constants are calculated with the help of Eqs. (16) and (17), and their time evolutions are shown in Fig. 5. The figure shows that, for all Reynolds numbers, c_0 approaches a constant value directly after the initial transient; it remains constant as long as there is sufficient turbulence, even though this period is only very short for the two cases with the lowest Reynolds numbers. For these cases, an increase of the constant c_0 is already observed before $t/T = 10$, because of the effects of viscosity. The value of c_0 decreases with increasing Reynolds number, but convergence emerges for the highest Reynolds numbers, even though small differences between ReL and ReXL remain visible. To scale our results, we choose a value of 0.145 for c_0 based on simulation ReXL. This value is in the range of 0.14 to 0.16 that has been presented in Beljaars (1995, his Fig. 2) and Mellado et al. (2015). Constant c_1 has been determined by trial and error to ensure that the time series $\min(\langle b \rangle) h_{*_m}^{-1} N^{-2}$ becomes constant in time. Also, constant c_1 displays Reynolds number dependence, mostly related to the dependence of the near-surface mean buoyancy profile on Reynolds number. A similar conclusion is drawn from the large-eddy simulations by Sullivan and Patton (2011, their Fig. 2), who show that in the mean potential temperature profile the thicknesses of the surface layer and the entrainment zone decrease with increasing resolution, thus with increasing effective Reynolds number. We have inferred a value of 1.026 for c_1. To predict the kinetic energy, we define two more constants c_e and c_B that relate the vertically integrated kinetic energy, buoyancy, and dissipation to the model variables following:

$$I_e = c_e h_{*_m} w_{*_m}^2, \tag{30}$$

$$I_{B,\varepsilon} = c_B h_{*_m} B_{sm}. \tag{31}$$

The constants calculated from the model results are $c_e = 0.5$ and $c_B = 0.46$, based on the data from simulation ReL.

6. Scaling the results

a. Time evolution

The scaled time evolutions of the buoyancy- and kinetic-energy-related variables are shown in Fig. 6, which is similar to Fig. 2, but with the mathematical model used to normalize the results. For each of the variables, a constant value in time corresponds to a perfect performance of the model. Each of the results show a convergence toward the value predicted by the model with increasing Reynolds numbers, and for all plotted variables there is convergence for simulations ReL and ReXL.

We can conclude from the time evolution of scaled surface buoyancy flux $\langle B_s \rangle / B_{sm}$ that our proposed model works very well as long as the Reynolds number is high enough but that the influence of viscosity eventually

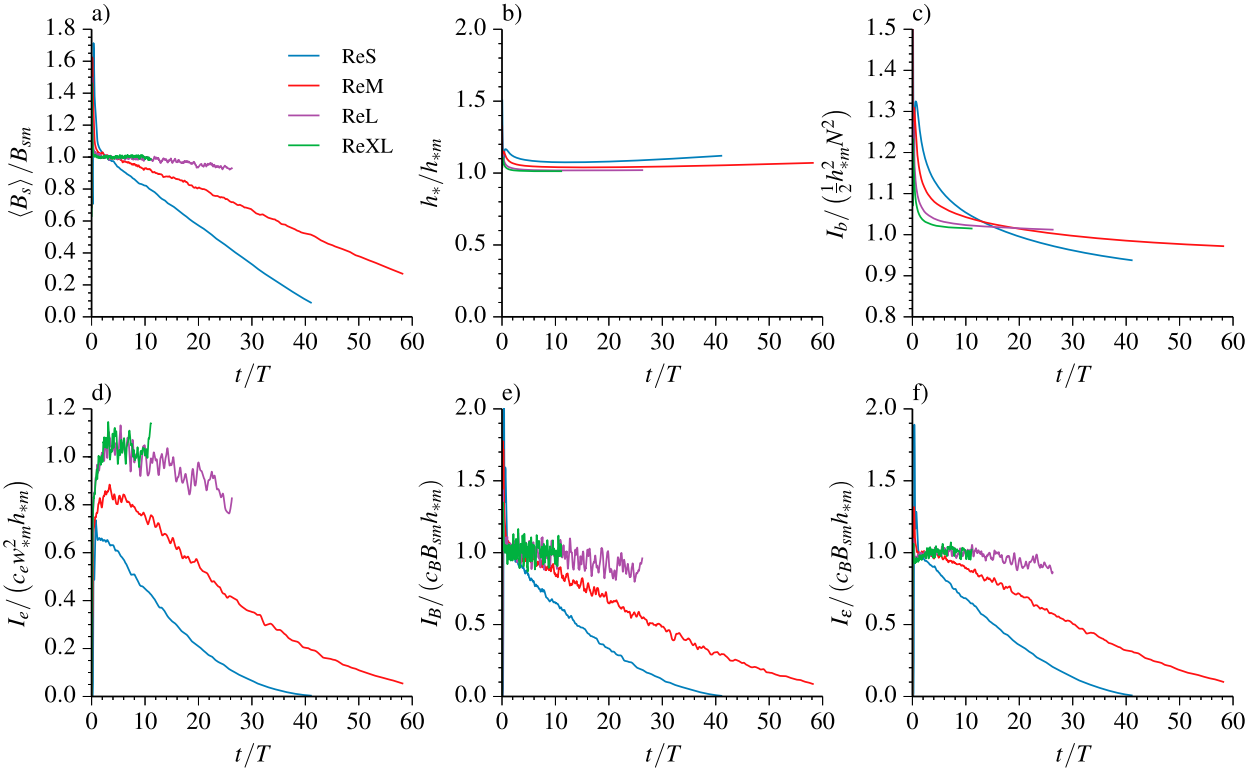

FIG. 6. (top) The scaled time evolution of (a) the mean surface buoyancy flux B_s, (b) the boundary layer height, and (c) the surface contribution to the vertically integrated buoyancy. (bottom) The scaled time evolution of (d) the vertically integrated kinetic energy, (e) buoyancy flux, and (f) dissipation.

causes a departure of the scaled variable from unity. The moment at which this happens is similar to the moment the top heating becomes relevant to the heat budget (see Fig. 2c). Top heating causes the gradient to reduce, resulting in a simulated surface flux that is less than the predicted flux and thus in a decrease of the scaled value in time. The lower importance of the top diffusion for larger Reynolds numbers can be observed well in Fig. 6c, where the evolution of the scaled surface contribution to the total heating starts following a constant line with increasing Reynolds number.

The height evolution (Fig. 6b) shows a scaled height h_*/h_{*_m} close to unity and convergence to exactly unity for increasing Reynolds number. This result shows that our chosen model [Eq. (18)] for the surface buoyancy flux provides the proper interaction with that of the height h_*, as the derived model predicts the length scale h_* very well.

The scaling of the kinetic-energy-related variables is more subtle. The model is able to predict the kinetic energy well (Fig. 6d), but the kinetic energy is sensitive to the correct prediction of the surface buoyancy flux; it drops quickly as soon as $\langle B_s \rangle / B_{sm}$ falls below unity, because the predicted surface buoyancy flux is too large. Figures 6e and 6f show that the model is well able to predict the buoyancy flux and the dissipation. As the time evolution of the kinetic energy (Fig. 6d) is the result of the delicate balance between buoyancy production and dissipation, more fluctuation is observed in this variable. Until a nondimensional time of 20, the model has at most 10% error, but subsequently the influence of viscosity increases the error beyond that.

b. *Profiles*

In Fig. 7, we present scaled vertical profiles of relevant buoyancy- and kinetic-energy-related variables, making use of the scaling variables provided by the derived model. The profiles are taken at equal intervals in the range where the nondimensional time of the system t/T varies between 1 and 8. The buoyancy profiles (Fig. 7a) show an adequate height scaling that results in self-similar behavior for the three cases with the largest Reynolds numbers. In addition, the acquired buoyancy profiles in the two cases with the largest Reynolds numbers collapse well, which shows that Reynolds number independence also applies to the shape of the profiles.

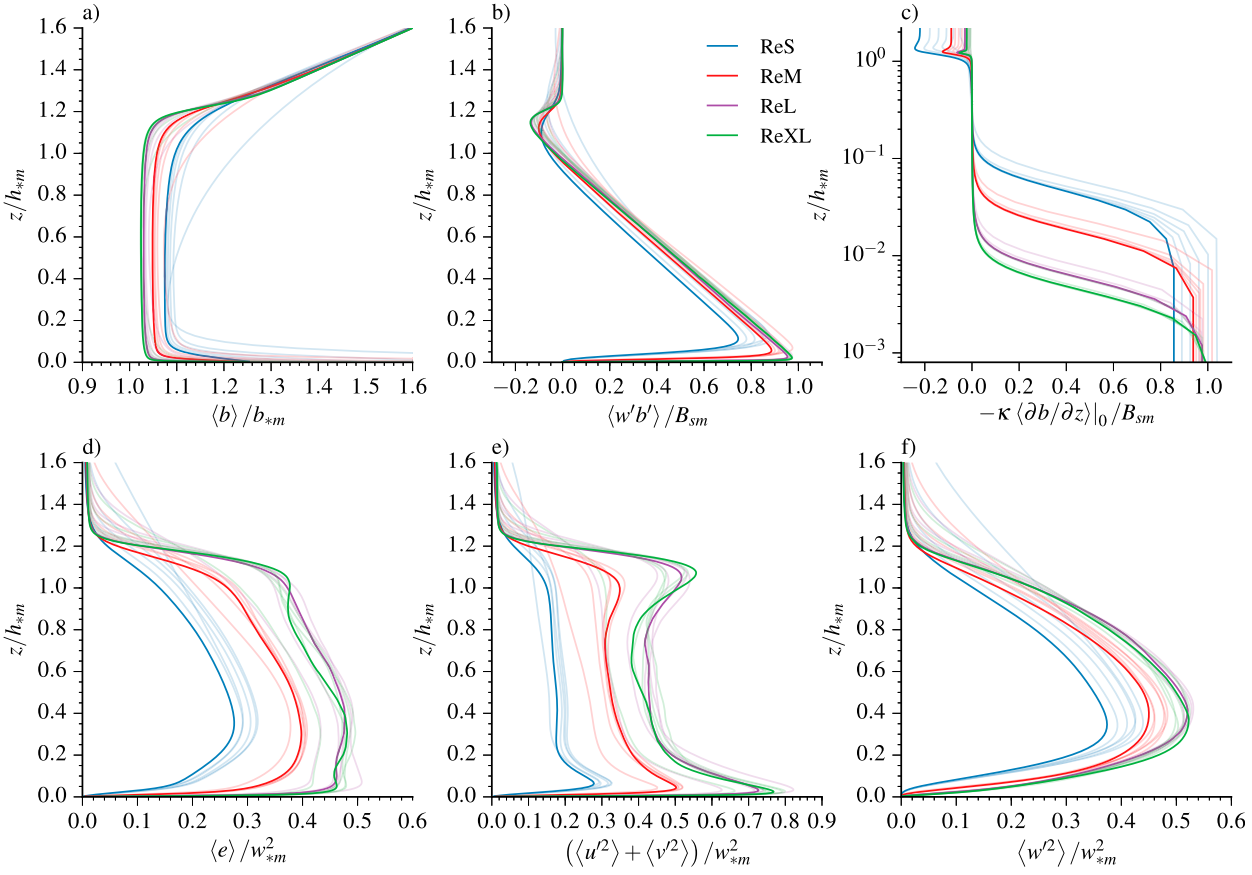

FIG. 7. Vertical profiles of (a) horizontally averaged buoyancy $\langle b\rangle$, (b) the buoyancy flux B, (c) the diffusive buoyancy flux, (d) the kinetic energy, (e) the horizontal velocity variance, and (f) the vertical velocity variance. The lines represent equal parts of the interval $t/T = 1$–8. Later times have darker colors.

Similar conclusions can be drawn from the profiles of the mean buoyancy flux $\langle w'b'\rangle$ (Fig. 7b). The three cases with the largest Reynolds numbers display a self-similar flux profile and the two with the largest value show identical profile shapes. The flux profiles show that the modeled flux B_{sm} is not the proper scaling variable for the two low–Reynolds number cases. The vertical profile of the viscous flux (Fig. 7c) shows that the scaled surface viscous buoyancy flux is decreasing in time for these two cases. We can infer from these results that, only for simulations ReL and ReXL, the viscous term in Eq. (9) can be neglected; thus, only for these cases, Eq. (20) is a good model.

The vertical profiles of the kinetic energy and the velocity variances show that the Reynolds number of the flow has a much larger impact on the kinetic-energy-related flow properties than on the thermodynamic characteristics of the flow. In Fig. 2, which displayed the time evolution of the vertically integrated mean kinetic energy, we found that the total normalized kinetic energy roughly doubles from the lowest to the highest Reynolds number. Figures 7d–f shows that the increase in kinetic energy with larger Reynolds numbers comes with a change in the shape of the profiles, where the two largest Reynolds numbers recover the profiles with the shape and magnitudes, exactly as those in Sullivan and Patton (2011, their Fig. 6). Note the conversion factor $w_*^2 = (h/h_{*_m})^{2/3} w_{*_m}^2 = (1.24)^{2/3} w_{*_m}^2$ between our results and those of Sullivan and Patton (2011) [the value of 1.24 originates from Garcia and Mellado (2014, their Table 2)]. We do not observe a relative loss of decay in kinetic energy near the top of the CBL in the early stages of decay, nor a relative increase in the final stages, as has been observed by Darbieu et al. (2015). In their study, the presence of shear in the early stages leads to a relative increase in kinetic energy near the surface, because the shear production is maintained by the large-scale pressure gradient, whereas the buoyancy production slowly decreases. In the final stages, the surface wind has largely ceased, and the shear that is still present in the higher regions of the boundary layer that are decoupled from the surface becomes the dominant production

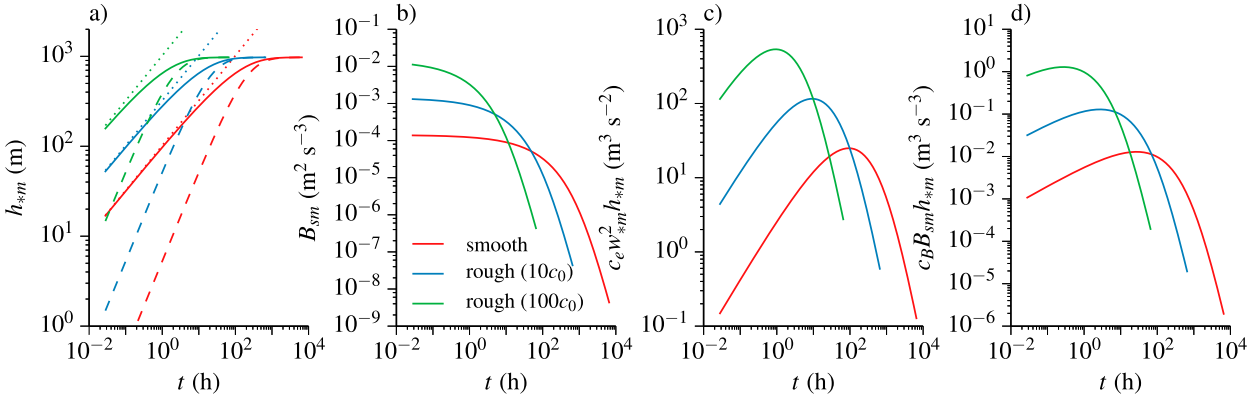

FIG. 8. Time evolution of (a) the CBL depth, (b) the surface buoyancy flux, (c) the vertically integrated kinetic energy, and (d) the vertically integrated buoyancy flux as predicted by the model described in section 5. The three lines represent three cases: the smooth flow with the original value of c_0, a factor-of-10 increase in c_0, and a factor-of-100 increase in c_0. The dashed and dotted lines in (a) represent the approximate solutions given in Eqs. (26) and (29), respectively.

term. As all forms of shear production are absent in our study, we observe a self-similar vertical profile of kinetic energy over the entire decay. All in all, the time evolution of vertical profiles remains a controversial topic, as consistent behavior did not emerge from intensive field campaigns yet (Grimsdell and Angevine 2002; Lothon et al. 2014).

To conclude, the analysis of the vertical profiles of buoyancy and velocity variances validates the applicability of our mathematical model for the scaling of high–Reynolds number simulations. Furthermore, it shows that, even though the integrated kinetic energy exhibits a complex time evolution, the vertical profiles display self-similarity. The Reynolds number similarity displayed in the two cases with the highest Reynolds numbers encourages the use of direct numerical simulation as a tool in atmospheric turbulence, as the required resolution to recover converged results from large-eddy simulations is only marginally higher [Sullivan and Patton (2011) found similarly converged results at 512^3 grid points] and the entire uncertainty introduced by subfilter-scale models has been eliminated.

7. Discussion: Roughness and decay during the afternoon transition

In the previous sections, we have validated the derived characteristic scales and the mathematical model for the bulk characteristics of the CBL and several kinetic-energy-related variables and have shown the presence of Reynolds number similarity. This allows us to extrapolate the results to the atmospheric boundary layer with very high Reynolds number. In this section, we use the mathematical model to analyze the time evolution of the system under typical atmospheric conditions. We have chosen here for an excess temperature of 6 K, a lapse rate of 0.006 K m^{-1}, a thermal diffusivity of 1×10^{-5} m^2 s^{-1}, and a buoyancy parameter g/θ_0 of 9.81/273 m s^{-2} K^{-1}.

One important difference between our experiments and most atmospheric flows is the type of bottom boundary, as nearly all atmospheric flows are rough. Zilitinkevich et al. (2006) and Beljaars (1995) have shown that free convection over rough surfaces is a delicate issue and that full understanding is still lacking. Nonetheless, Zilitinkevich et al. (2006) has estimated that, over a rough surface, the transfer coefficient can increase two orders of magnitude compared to a smooth surface. To study the time scales in an approximate atmospheric setting, we have calculated the time evolution of the system using the fitted constant c_0, representing the smooth surface, and with constants that are respectively one and two orders of magnitude higher, representing the rough surfaces. Assuming that we are studying dry systems, the initial surfaces fluxes with the chosen dimensions are 5, 50, and 500 W m^{-2}. All three are shown in Fig. 8.

According to the scaling laws, the rate of change of the system is proportional to $\langle B_s \rangle$ and thus to c_0. Based on the chosen values for c_0, the systems with rough surfaces evolve therefore 10 or 100 times faster than that with a smooth surface. With respect to atmospheric time scales, this difference is of great importance. Over a smooth wall, the height evolution can be well approximated using a fixed flux boundary condition for approximately 10 h, whereas for the roughest surface the solid and dotted lines depart from each other within a few minutes (Fig. 8a). Such information is relevant, for instance, to parameterizations that describe the refreezing of Arctic

leads; if the time it takes to refreeze a lead is within the time that the constant flux approximation is valid, it potentially allows for very simple models to describe the process. This finding can be directly related to the relative rate of change of the surface buoyancy flux since the initial value, shown in Fig. 8b, where the time during which the surface buoyancy flux is approximately constant, quickly reduces with increasing roughness. The time evolution of the integrated kinetic energy and buoyancy flux (Figs. 8c and 8d) show that the change in surface conditions can change the moment at which the peaks in integrated kinetic energy and buoyancy occur from values around 100 to approximately 1 h.

The linear dependence of the time scales in our system on the buoyancy transfer rate makes the surface model a crucial, and potentially overlooked, model component under conditions of free convection. The exact behavior of free convection over a rough surface is still not fully understood, although adequate parameterizations for large-scale models have been developed (Beljaars 1995). These solutions, however, are not applicable in large-eddy simulations, where the large-scale motions of the size of the CBL depth are resolved. Zilitinkevich et al. (2006) have made the case that, in regions of horizontal flow toward plumes, Monin–Obukhov-like parameterizations are applicable. However, few measurement data are available, and the solution to this problem remains incomplete. Consequently, large-eddy simulations of (cloudy) boundary layers over sea surfaces may exhibit an important dependence on the chosen formulation of the surface model and the way roughness is accounted for during free convection.

With respect to the decay of turbulence during the afternoon transition, our results indicate that, at atmospheric Reynolds numbers, the quasi-steady state, thus the dominant balance between the buoyancy flux and dissipation, can be maintained until the input of energy from the surface buoyancy flux has nearly vanished. Van Driel and Jonker (2011) have shown that this balance holds for systems that have slow fluctuations in the surface buoyancy flux, although they worked with prescribed fluxes. As a result of this balance, the time evolution of the kinetic energy in the system can be excellently predicted from the solution of Eq. (10), as long as the appropriate model for B_s is provided and this variable does not vary too rapidly. The time evolution of integrated kinetic energy cannot be approximated by a power law, nor by an exponential function, but is dependent on the shape of the specified function for B_s. This finding suggests that the power-law decay of integrated kinetic energy found by Nieuwstadt and Brost (1986) after a sudden stop of energy input at the bottom is not a good basis for the study of the decay of turbulence during the afternoon transition. Our results explain, for instance, why Sorbjan (1997, line D1 in his Fig. 2) and Nadeau et al. (2011, their Fig. 7) do not find a region with a constant power law, but instead an increasingly negative slope, in agreement with our Fig. 8c. In case a sinusoidal heat flux profile with a period that matches the diurnal cycle is prescribed for B_s, also an accelerating decay is found (not shown). The power law is therefore not an artifact of the characteristic shape of the daily evolution of the surface buoyancy flux.

8. Conclusions

We have characterized the growth and decay of a convective boundary layer (CBL) over a surface with a constant surface temperature and a linear stratification. This system has only the Reynolds and Prandtl numbers as nondimensional parameters. We have done direct numerical simulations for four different Reynolds numbers and have chosen a Prandtl number of unity for all simulations. We have derived a mathematical model that describes the time evolution of the buoyancy- and velocity-variance-related variables and verified the model against the simulations.

Each simulation has a decaying surface buoyancy flux from the beginning, because the temperature difference between the surface and the atmosphere is decreasing. However, the vertically integrated kinetic energy, buoyancy flux, and dissipation initially increase in time, because the contribution of boundary layer growth is more important than the decay of the flux. These variables develop toward a peak and decay subsequently. The derived model is very well able to describe the evolution of the bulk variables of high–Reynolds number flows. Our simulations display Reynolds number similarity for the two cases with the highest Reynolds numbers, which suggests that our results can be extrapolated to the atmosphere, despite their moderate Reynolds numbers. This demonstrates the applicability of direct numerical simulation to the study of atmospheric boundary layers.

The time rate of change of the system is linearly related to the surface flux of buoyancy, and therefore any atmospheric model study depends crucially on correctness of the mathematical formulation of the surface model. Especially in large-eddy simulations over water surfaces, which is a common setting for studies of cloudy boundary layers, the importance of the chosen surface roughness may have been underestimated. Even in the case of a friction-velocity-dependent roughness (Charnock 1955), an arbitrary constant is involved that has a large influence on the time scale of the system. We, however, cannot give the definitive answer on the role of

surface roughness in free convection, which warrants a repetition of this study, but with a rough surface implemented at the bottom boundary.

This system can be seen as a limiting case for the decay of turbulence during the afternoon transition, as the surface flux slowly develops toward a value of zero. Our results show that the evolution of kinetic energy in the decay phase is not exponential, nor does it follow a power law, as a result of the competing effects of boundary layer growth and a decreasing surface flux. The derived model in this paper is able to predict the correct evolution in time of the CBL depth, kinetic energy, buoyancy production, and dissipation.

Acknowledgments. Support from the Max Planck Society through its Max Planck Research Groups program is acknowledged. Computational resources were provided by the Jülich Supercomputing Centre. We acknowledge Alberto De Lozar for the discussions on the scaling of the data and Antoon van Hooft for his useful comments on the paper.

REFERENCES

Beljaars, A. C. M., 1995: The parametrization of surface fluxes in large-scale models under free convection. *Quart. J. Roy. Meteor. Soc.*, **121**, 255–270, doi:10.1002/qj.49712152203.

Charnock, H., 1955: Wind stress on a water surface. *Quart. J. Roy. Meteor. Soc.*, **81**, 639–640, doi:10.1002/qj.49708135027.

Darbieu, C., and Coauthors, 2015: Turbulence vertical structure of the boundary layer during the afternoon transition. *Atmos. Chem. Phys.*, **15**, 10 071–10 086, doi:10.5194/acp-15-10071-2015.

Deardorff, J. W., 1970: Convective velocity and temperature scales for the unstable planetary boundary layer and for Rayleigh convection. *J. Atmos. Sci.*, **27**, 1211–1213, doi:10.1175/1520-0469(1970)027<1211:CVATSF>2.0.CO;2.

——, G. E. Willis, and D. K. Lilly, 1969: Laboratory investigation of non-steady penetrative convection. *J. Fluid Mech.*, **35**, 7–31, doi:10.1017/S0022112069000942.

Dimotakis, P. E., 2000: The mixing transition in turbulent flows. *J. Fluid Mech.*, **409**, 69–98, doi:10.1017/S0022112099007946.

Esau, I., 2007: Amplification of turbulent exchange over wide Arctic leads: Large-eddy simulation study. *J. Geophys. Res.*, **112**, D08109, doi:10.1029/2006JD007225.

Fedorovich, E., 1995: Modeling the atmospheric convective boundary layer within a zero-order jump approach: An extended theoretical framework. *J. Atmos. Sci.*, **34**, 1916–1928, doi:10.1175/1520-0450(1995)034<1916:MTACBL>2.0.CO;2.

Garcia, J. R., and J. P. Mellado, 2014: The two-layer structure of the entrainment zone in the convective boundary layer. *J. Atmos. Sci.*, 1935–1955, doi:10.1175/JAS-D-13-0148.1.

Grimsdell, A. W., and W. M. Angevine, 2002: Observations of the afternoon transition of the convective boundary layer. *J. Appl. Meteor.*, **41**, 3–11, doi:10.1175/1520-0450(2002)041<0003:OOTATO>2.0.CO;2.

Lothon, M., and Coauthors, 2014: The BLLAST field experiment: Boundary-layer late afternoon and sunset turbulence. *Atmos. Chem. Phys.*, **14**, 10 931–10 960, doi:10.5194/acp-14-10931-2014.

Mellado, J. P., 2012: Direct numerical simulation of free convection over a heated plate. *J. Fluid Mech.*, **712**, 418–450, doi:10.1017/jfm.2012.428.

——, C. C. van Heerwaarden, and J. R. Garcia, 2015: Near-surface effects of stratification above a free convective boundary layer. *Bound.-Layer Meteor.*, **159**, 69–95, doi:10.1007/s10546-015-0105-x.

Moeng, C. H., 1984: A large-eddy simulation for the study of planetary boundary layer turbulence. *J. Atmos. Sci.*, **41**, 2052–2062, doi:10.1175/1520-0469(1984)041<2052:ALESMF>2.0.CO;2.

Morinishi, Y., T. S. Lund, O. V. Vasilyev, and P. Moin, 1998: Fully conservative higher order finite difference schemes for incompressible flow. *J. Comput. Phys.*, **143**, 90–124, doi:10.1006/jcph.1998.5962.

Nadeau, D. F., E. R. Pardyjak, C. W. Higgins, H. J. S. Fernando, and M. B. Parlange, 2011: A simple model for the afternoon and early evening decay of convective turbulence over different land surfaces. *Bound.-Layer Meteor.*, **141**, 301–324, doi:10.1007/s10546-011-9645-x.

Nieuwstadt, F. T. M., and R. A. Brost, 1986: The decay of convective turbulence. *J. Atmos. Sci.*, **43**, 532–546, doi:10.1175/1520-0469(1986)043<0532:TDOCT>2.0.CO;2.

Pope, S. B., 2000: *Turbulent Flows.* Cambridge University Press, 802 pp.

Sorbjan, Z., 1997: Decay of convective turbulence revisited. *Bound.-Layer Meteor.*, **82**, 503–517, doi:10.1023/A:1000231524314.

Sullivan, P. P., and E. G. Patton, 2011: The effect of mesh resolution on convective boundary layer statistics and structures generated by large-eddy simulation. *J. Atmos. Sci.*, **68**, 2395–2415, doi:10.1175/JAS-D-10-05010.1.

——, C. H. Moeng, B. Stevens, D. Lenschow, and S. D. Mayor, 1998: Structure of the entrainment zone capping the convective atmospheric boundary layer. *J. Atmos. Sci.*, **55**, 3042–3064, doi:10.1175/1520-0469(1998)055<3042:SOTEZC>2.0.CO;2.

Tompkins, A. M., and G. C. Craig, 1998: Time-scales of adjustment to radiative-convective equilibrium in the tropical atmosphere. *Quart. J. Roy. Meteor. Soc.*, **124**, 2693–2713, doi:10.1002/qj.49712455208.

Townsend, A. A., 1959: Temperature fluctuations over a heated horizontal surface. *J. Fluid Mech.*, **5**, 209–241, doi:10.1017/S0022112059000167.

van Driel, R., and H. J. J. Jonker, 2011: Convective boundary layers driven by nonstationary surface heat fluxes. *J. Atmos. Sci.*, **68**, 727–738, doi:10.1175/2010JAS3643.1.

vanZanten, M. C., and Coauthors, 2011: Controls on precipitation and cloudiness in simulations of trade-wind cumulus as observed during RICO. *J. Adv. Model. Earth Syst.*, **3**, M06001, doi:10.1029/2011MS000056.

Vasilyev, O. V., 2000: High order finite difference schemes on non-uniform meshes with good conservation properties. *J. Comput. Phys.*, **157**, 746–761, doi:10.1006/jcph.1999.6398.

Williamson, J. H., 1980: Low-storage Runge-Kutta schemes. *J. Comput. Phys.*, **35**, 48–56, doi:10.1016/0021-9991(80)90033-9.

Zilitinkevich, S. S., 1991: *Turbulent Penetrative Convection.* Avebury, 199 pp.

——, and Coauthors, 2006: The influence of large convective eddies on the surface-layer turbulence. *Quart. J. Roy. Meteor. Soc.*, **132**, 1423–1456, doi:10.1256/qj.05.79.